Article

Effect of Dy³⁺ Amount on the Structural and Luminescence Properties of LaNbO₄:Dy³⁺ Phosphor Obtained by One-Step Spray Pyrolysis Process

Gabriela S. Freiria,[a] Amanda L. Ribeiro,[a] Marc Verelst,[b] Eduardo J. Nassar,[a] and Lucas A. Rocha[a]*

[a]*Departamento de Química, Universidade de Franca (UNIFRAN),
CP 82, 14404-600 Franca-SP, Brazil*

[b]*Centre d'Elaboration de Matériaux et d'Etudes Structurales (CNRS),
BP 4347, 31055 Toulouse CEDEX 4, France*

In this study, Dy³⁺-doped LaNbO₄ phosphors with a blue to white emission that can be tuned by varying the activator concentration were prepared by one-step spray pyrolysis process. According to the powder X-ray diffraction results, increasing Dy³⁺ concentration favored the tetragonal phase. Slight changes were observed in the recorded Raman spectra as a function of Dy³⁺ concentrations while SEM (scanning electron microscopy) micrographs presented similar profiles regardless the Dy³⁺ amount. Investigation of Dy³⁺ emission data in the visible range showed that rising the Dy³⁺ concentration progressively shifted the emission towards the white color. All samples presented a wide excitation range from 254 to 475 nm.

Keywords: spray pyrolysis, luminescence, lanthanum niobate

Introduction

Over the last years, rare earth ions (RE³⁺) have received increasing attention: solid-state materials doped with these ions can be applied in color screens, lighting, and optical devices.[1-5] The luminescence properties of these materials heavily depend on the structure of the electron energy levels. In RE³⁺, chemical binding affects these levels very little because orbitals 5s and 5p shield orbital 4f efficiently.[6] The f-f transitions in RE³⁺ cause an array of emissions at different wavelengths, giving rise to a plethora of colors. However, f-f transitions are forbidden by the parity selection rule (Laporte rule), so they have low excitation efficiency. Excitation requires the use of a matrix and/or sensitizer that is able to absorb energy and transfer it to an emitting ion.[6,7]

Lanthanum niobate (LaNbO₄) is a promising material for multifunctional applications. It has a band-gap of approximately 4.8 eV and emits blue and ultraviolet light when excited with ultraviolet (UV) radiation and X-rays, respectively.[8,9] Moreover, LaNbO₄ can transfer the absorbed energy to other emitting species, leading to different fluorescence emissions.[10,11] This oxide has been prepared by a number of techniques; for example,

spray pyrolysis (SP),[12-14] solid-state reaction,[15-17] reactions in solution[18-20] and sol-gel route.[10,21] However, with an exception of our previously published work,[22] the authors were not able to finely control the size, shape, and distribution properties. Moreover, the SP process is completed in only several seconds, while other currently available methods require several hours or days to complete the process, even requiring a post annealing treatment. Briefly, SP process involves the vaporization of precursor solution followed by the drying, precipitation and decomposition in heated tubular furnace reactors. The stoichiometric ratio in the final prepared material is the same as the precursor solution, since the reaction and aggregation volume are confined in each generated micrometric droplet, which can be seen as a micro reactor. Therefore, particles synthesized by the SP process can be obtained on a laboratory or on an industrial scale.[22-25]

Among the various materials doped with lanthanide ions (Ln³⁺) reported in the literature, nanomaterials doped with Dy³⁺ are rarely mentioned as compared to the other Ln³⁺. Dy³⁺ easily reaches the maximum concentration (quenching), and the nature of the host matrix strongly influences emission from this ion. When Dy³⁺ is excited with UV or blue light, their emission profile is characterized by the emergence of three narrow bands in the visible

region, as follows: (*i*) a band in the blue region near 485 nm, corresponding to the magnetic dipole transition $^4F_{9/2} \rightarrow {}^6H_{15/2}$; (*ii*) a band in the yellow region around 575 nm, due to electric dipole transition $^4F_{9/2} \rightarrow {}^6H_{13/2}$ hypersensitive to the crystalline field; and (*iii*) a weak band in the red region near 665 nm, referring to the transition $^4F_{9/2} \rightarrow {}^6H_{11/2}$. Therefore, pure white light can be produced by adjusting the intensities of the integrals of the emission areas in the yellow and blue regions. Furthermore, Dy^{3+} displays multiple emissions in the near infrared region, which is an important feature for application in telecommunications.[6,26-31]

Great efforts have been made to obtain phosphors that can emit white light. These phosphors could be applied in light-emitting diodes (W-LEDs), which in turn could be used in numerous areas. W-LEDs are considered as a new source of light emitters in the solid state and offer many advantages like small volume, high efficiency, long lifetime, low energy consumption, and lack of toxicity, which make them environmentally friendly. There are several ways to obtain white light, including the use of LED comprising three chips capable of emitting red, green, and blue (RGB) light.

Recently, attention has been devoted to the synthesis of stable, single phosphors doped with RE^{3+}, such as $K_2Y(WO_4)(PO_4):Tm^{3+}$, Dy^{3+},[32] $Ca_2PO_4Cl:Dy^{3+}$,[33] $Ca_3Y(GaO)_3(BO_3)_4:Ce^{3+}$, Mn^{2+}, and Tb^{3+},[34] which present higher light efficiency and do not undergo phase separation. These features are difficult to obtain in LEDs consisting of more than one phosphor. Single phosphors avoid issues related to low light efficiency due to reabsorption between phosphors and color degradation due to the different degradation rates of each individual phosphor. In this work we described the effect of Dy^{3+} concentration on the emission color of $LaNbO_4:Dy^{3+}$ phosphor obtained by spray pyrolysis.

Experimental

Dy_2O_3 and La_2O_3 were acquired from Sigma-Aldrich and calcined at 900 °C for 2 h. Next, they were dissolved in HCl 6.0 mol L^{-1} to obtain Dy^{3+} and La^{3+} at 1.10×10^{-1} and 5.10×10^{-1} mol L^{-1}, respectively. NbCl$_5$ was donated by Companhia Brasileira de Metalurgia e Mineração (CBMM).

LaNbO$_4$ doped with Dy^{3+} ions

The $LaNbO_4$ matrices were doped with different concentrations of Dy^{3+} ions, to obtain $La_{(100\% - x)}Dy_{(x)}NbO_4$, where $0.25 \leq x \leq 15.0\%$ in moles. The obtained samples containing 0.25, 0.5, 1.0, 3.0, 5.0, 10.0 and 15.0% in moles

of Dy^{3+} ion were called A, B, C, D, E, F and G, respectively. The phosphors were prepared as follows:[22,23,35] first, Dy^{3+} and La^{3+} were added to an aqueous solution containing NbCl$_5$ (pH = 2.0, hydrochloric acid) obtaining a final concentration of 0.14 mol L^{-1}. After homogenization, the solution was placed in the aerosol pyrolysis system. Nebulization was achieved by using a piezoelectric pellet (2.4 MHz). The resulting aerosol was carried through the system at a constant flow (2.0 mL min^{-1}); it passed through the drying region (100 °C) and then through the decomposition region (900 °C). Finally, the resulting powder was collected with the aid of an electrostatic filter operating with a potential gradient of 11 kV.

Characterization

Powder X-ray diffraction analysis (XRD) was performed at room temperature on a Rigaku Geigerflex D/max-c diffractometer operating with monochromated CuKα radiation (λ = 1.54 Å). Diffractograms were recorded in the 2θ range from 10 to 80° at a resolution of 0.05°. Particle morphology was investigated by scanning electron microscopy (SEM) on a Shimadzu microscope model VEGA 3 SB. Raman spectroscopy was conducted on a Micro-Raman Jobin Yvon Horiba Spex spectrometer. The spectra were recorded from 100 to 1,200 cm^{-1}, in two cycles. Excitation was accomplished with a He-Ne laser at 632.8 nm. The photoluminescence data were obtained at room temperature, under continuous Xe lamp (450 W) excitation in a Horiba Jobin Yvon Fluorolog-3 spectrofluorimeter equipped with an excitation and emission double monochromator and a photomultiplier R 928 Hamamatsu. The emission was collected at 90° from the excitation beam. The slits were placed at 2.0 and 0.5 nm for excitation and emission, respectively; the bandpass was 0.5 nm, and the integration time was 0.5 ms. G1227 emission filters were employed (transmittance 100% for λ > 450 nm). All the analyses were carried out at room temperature.

Results and Discussion

Powder X-ray diffraction analysis (XRD)

Figure 1a shows the powder X-ray diffractograms of the $La_{(100\% - x)}Dy_{(x)}NbO_4$ matrices (x = 0.25-15.0% in moles) and the JCPDS standards. The diffractograms of all samples displayed the typical peaks of a crystalline material, identified as the monoclinic phase of $LaNbO_4$ (JCPDS 22-1125) with spatial group I2 and unit cell parameters a = 5.567, b = 11.52, and c = 5.205 Å and/or as the tetragonal phase (JCPDS 50-919) with spatial group I and unit cell

parameters a = 5.35 and c = 11.53 Å. The crystal sizes were estimated using the Scherrer formula[21] and the values obtained were similar for all samples. For the diffraction plane h k l (–1 2 1) at $2\theta = 27.58°$ related to the monoclinic phase, the mean crystal size was about 12.9 nm, while for the diffraction plane (1 1 2) at $2\theta = 28.14°$ related to the tetragonal phase, the mean value found was about 29.1 nm.

Increasing Dy³⁺ concentration favored formation of the tetragonal phase (JCPDS 50-919): the peaks due to the monoclinic phase ($2\theta = 27$ and 29°) decreased for samples E, F, and G, whereas the peak at $2\theta = 28°$, typical of the tetragonal phase, intensified. Figure 1b shows an illustration of the crystal structures of LaNbO₄ created using VESTA software[36] and the percentage of the tetragonal phase in function of Dy³⁺ concentration.

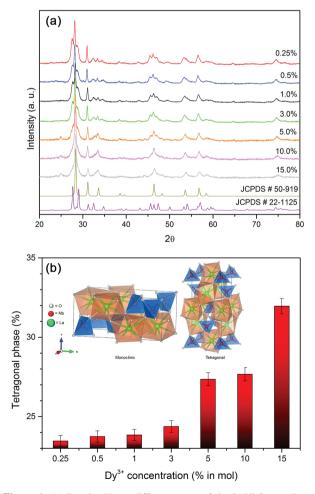According to Nico *et al.*,[37] the rare earth niobates (RENbO₄) are known to crystallize in a fergusonite-type structure, i.e., in a monoclinic structure (space group C₂ₕ⁶), undergoing a pure and reversible ferroelastic phase transformation to a scheelite-type structure, with a tetragonal system lattice (space group C₄ₕ⁶). In the monoclinic phase the Nb and RE atoms occupy the Wyckoff positions 4e while the O atoms occupy the 8f position, in the NbO₆ octahedra. The tetragonal phase is not built on NbO₆ octahedra, but instead on unlinked NbO₄ tetrahedra with the RE, Nb and O atoms occupying, individually and respectively, the 4b, 4a and 16f Wyckoff positions. The lattice parameters of the RENbO₄ compounds will obviously depend on the lanthanide ion. Rooksby and White[38] reported that by comparing the values of the lattice parameters of the two structures (monoclinic and tetragonal) the transition is seen to be equivalent to a removal of a monoclinic distortion of the tetragonal scheelite-type structure. At the transition point, the monoclinic β angle is decreased to 90°, the monoclinic a and c parameters reach equality to give the tetragonal a parameter, and the monoclinic b parameter becomes the c parameter of the tetragonal cell. Thus, it is therefore possible that the monoclinic distortion might disappear by the increase of Dy³⁺ concentration due to the differences of ionic radius and atomic volume between La³⁺ (1.22 Å and 22.0 cm³ mol⁻¹) and Dy³⁺ (0.91 Å and 19.0 cm³ mol⁻¹), respectively.

Raman spectroscopy

Raman spectroscopy helped to observe changes in the crystalline structure of the matrix as a function of the Dy³⁺ concentration. Figure 2 illustrates the Raman spectra between 50 and 1200 cm⁻¹ of the undoped and (Dy³⁺)-doped samples synthesized at 900 °C. The bands at 107, 196, and 421 cm⁻¹ were ascribed to La–O vibrations.[21,39-41] The bands between 50 and 120 cm⁻¹ referred to vibrations of octahedron as a whole. The bands between 150 and 400 cm⁻¹ corresponded to vibrations of cations localized inside octahedral and tetrahedral sites. The bands at higher wavelength, between 500 and 1000 cm⁻¹, were assigned to stretching of the covalent Nb–O bonds in NbO₄.[42,43]

As a result of the changes in Dy³⁺ concentration, the full width at half maximum (FWHM) increased for some bands, especially for the band at 803 cm⁻¹. FWHM values went from 12.81 nm (sample A) to 21.71 nm (sample F) because Dy³⁺ replaced La³⁺, which affected the rigidity of the NbO₄ tetrahedron. The band at 985 cm⁻¹ was attributed to asymmetric stretching of Nb=O bonds.[21]

Scanning electron microscopy (SEM)

Figure 3 presents the SEM micrographs for all samples. The Dy³⁺ variation did not affect the particle morphology or
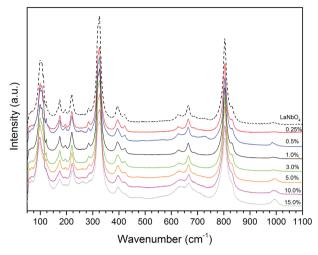

Figure 1. (a) Powder X-ray diffractograms of the LaNbO₄ matrices containing different Dy³⁺ ions concentrations and the JCPDS standards; and (b) the percentage of the tetragonal phase. Inset: crystal structures of LaNbO₄. The niobium polyhedrons are represented in blue whereas the lanthanum polyhedrons in orange.

Figure 2. Raman spectra of undoped and (Dy³⁺)-LaNbO₄ samples containing different Dy³⁺ concentrations.

the size distribution of the samples, which were consisted of polydisperse spherical particles with sizes between 16 nm and 1.5 μm of diameter.[44] All the samples presented a bimodal size distribution, where the first group presented diameters below 200 nm while the second one exhibited a mean size of around 600 nm.

Figure 4 presents the size distributions and the correspondent SEM micrographs for the samples containing 5.0% of Dy³⁺ ions. In order to analyze the particle's diameter profile for the first group, this sample was centrifuged at 14,000 rpm during 5 min and then it was submitted to the SEM analysis, as shown in Figure 4b. As expected, all the particles presented sizes below 200 nm. It could be observed

that the centrifuged particles also exhibited a bimodal distribution profile with peaks at 28 and 78 nm. This fact is interesting due to the possibility of obtaining phosphors that present a wide range of applications in biomedical analysis, such as imaging or sensing.

Photoluminescence

Figure 5 contains the excitation and emission spectra and the decay curves for the undoped and (Dy³⁺)-LaNbO₄ samples. The excitation spectra (Figure 5a) show transitions from the ground state $^6H_{15/2}$ to the excited states $^6P_{3/2}$; $^4F_{5/2}$, $^4I_{9/2}$, $^4L_{9/2}$, and $^4H_{17/2}$; $^4M_{15/2}$, $^4I_{11/2}$, and $^6P_{7/2}$; $^6P_{5/2}$; $^4I_{13/2}$ and $^4F_{7/2}$; $^4G_{11/2}$; and $^4I_{15/2}$ occurred at 326, 338, 352, 366, 387, 427, and 449 nm, respectively.[45,46] The broad band at 254 nm in the excitation spectra corresponded to charge transfer band (CTB) from orbital 2p in oxygen to empty orbitals 4d and 4f in Nb⁵⁺ and Dy³⁺, respectively.[22,47] Furthermore, the samples presented a wide excitation range, including all the UV-LED and blue emission regions.

Figure 5b presents the spectra which were normalized by adopting the magnetic dipole transition $^4F_{9/2} \rightarrow {}^6H_{15/2}$ at 477 nm as reference.[29] Narrow bands emerged in the blue region with maximum at 477 nm ($^4F_{9/2} \rightarrow {}^6H_{15/2}$ transition), yellow region with maximum at 575 nm ($^4F_{9/2} \rightarrow {}^6H_{13/2}$ transition), and red region with maximum at 664 nm ($^4F_{9/2} \rightarrow {}^6H_{11/2}$ transition), which are typical of Dy³⁺ emission. The broad band between 400 and 480 nm was due to blue emission from the LaNbO₄ matrix. This band may have resulted from transition from orbital 2p of the
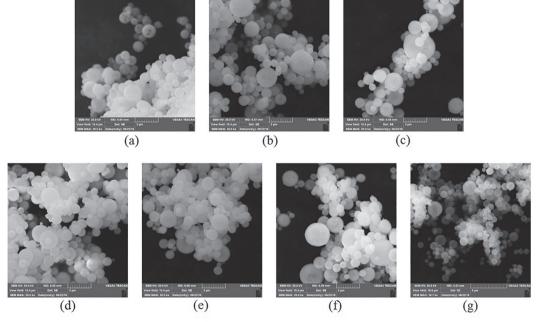

Figure 3. SEM images for all samples containing different Dy³⁺ concentrations: (a) 0.25%; (b) 0.5%; (c) 1.0%; (d) 3.0%; (e) 5.0%; (f) 10.0% and (g) 15.0% in moles of Dy³⁺ ion.
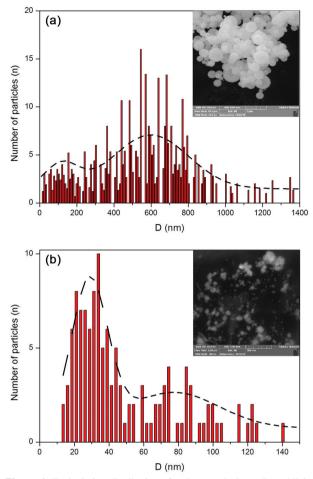
Figure 4. Typical size distributions for the sample La$_{(95.0)}$Dy$_{(5.0)}$NbO$_4$ (a) before and (b) after the centrifugation process. The lines are just a guide for the eyes (n = 320 and 130 particles analyzed, respectively). Inset: SEM image of the samples used in size distribution measurements.

ligand O^{2-} to the empty states of configuration 4f of Dy^{3+} (Dy$^{3+} \rightarrow$ O^{2-}) and 4d of the central niobium atom in NbO$_4$$^{3-}$ (Nb$^{5+} \rightarrow$ O^{2-}). The increase of Dy^{3+} concentration reduced the blue emission broad band attributed to the matrix and intensified the transition ^{4}F$_{9/2} \rightarrow$ ^{6}H$_{13/2}$ (575 nm).[22,47,48] The emission profiles of the samples excited at 352, 387, and 450 nm also displayed bands due to transitions related to Dy^{3+} (^{4}F$_{9/2} \rightarrow$ ^{6}H$_J$, J = 15/2, 13/2, and 11/2). Nevertheless, the band corresponding to the emission from the matrix decreased considerably which suggested that these excitation wavelengths favored the Dy^{3+} emission.

The decay curves of samples containing different Dy^{3+} concentration were collected, as shown in Figure 5c. The entire decay curves can be fitted to a mono-exponential decay model.[49] The obtained lifetimes monitored at 574 nm decrease from 0.50 to 0.28 ms, for the samples containing 0.25 and 15.0% of Dy^{3+} ion, suggesting the quenching by the Dy^{3+} concentration.[50,51] It was not possible to measure the lifetime for the undoped sample due to the technique parameters of the fluorescence equipment.
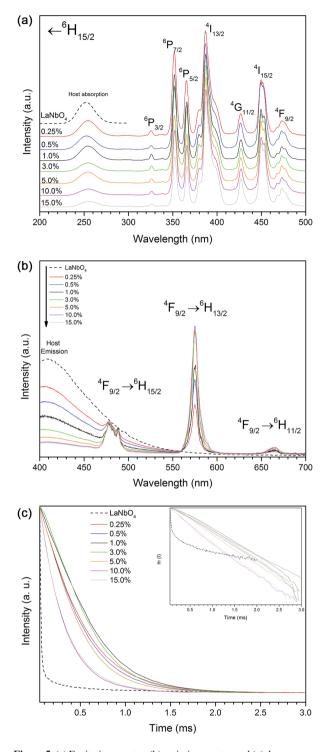

Figure 5. (a) Excitation spectra; (b) emission spectra and (c) decay curves of the undoped and (Dy^{3+})-LaNbO$_4$ samples. For the undoped sample, the excitation and emission wavelengths used were λ_{exc} = 254 nm and λ_{em} = 410 nm, while for the (Dy^{3+})-LaNbO$_4$ samples the wavelengths were λ_{exc} = 254 nm and λ_{em} = 575 nm.

The increase of activator concentration results in high luminescence intensity up to a certain maximum value, and then it decrease beyond that value. This effect has been named concentration quenching, which can occur as a result

of: (*i*) loss of excitation energy from the emitting state due to cross-relaxation between the activators; (*ii*) excitation migration owing to resonance between the activator ions and (*iii*) coagulated or paired activator ions acting as quenching center.[51] Furthermore, the optimum activator concentration depends on many variants, such as nature of the host matrix, number of lattice sites or neighbors and the activator.[51]

In order to confirm the nature of the broad band, the emission spectra were recorded at different time delays, as shown in Figure 6. The time-resolved spectra were obtained by reading the signal at time of 0.01-0.05 ms after the end of the excitation source. It could be observed that increasing both, the time delay and the Dy^{3+} ions concentration promote a continuous decreasing of the broad band intensity, which was totally eliminated at around 0.03 ms for samples with 1.0% or higher of Dy^{3+} ions concentrations.

The chromaticity coordinates (CIE) were obtained on the basis of the emission spectra recorded at room temperature for excitation at 254 nm. The Spectra Lux 2.0 program developed by Santa-Cruz and Teles[52] was used. Figure 7 and Table 1 show the CIE results and the figure also presents the picture showing the emission color of all samples under excitation of 254 nm. For the $LaNbO_4$ matrices, increasing Dy^{3+} concentration made the system gradually approach the coordinates in the white region upon excitation at 254 nm. As discussed previously, this fact occurs due to reduction of emission of the matrix in the blue region caused by the increases of the Dy^{3+} ions concentration.

The samples containing 3.0% or higher of Dy^{3+} amounts presented CIE coordinates closer to the white light emission standard (x = 0.33 and y = 0.33),[53] while the samples containing lower Dy^{3+} concentrations presented CIE coordinates in the blue region of the diagram.

Conclusions

In this work, $LaNbO_4$ phosphors doped with different Dy^{3+} concentrations were synthesized by the SP process, which presents many advantages in comparison to the usual processes. The materials show a tunable emission color from the blue to the white region with increasing amounts of Dy^{3+} ions. The nanospheres obtained show a bimodal distribution profile with high crystallinity. The luminescence spectra presented a wide range of excitation (254 to 475 nm) and the increase of Dy^{3+} concentration
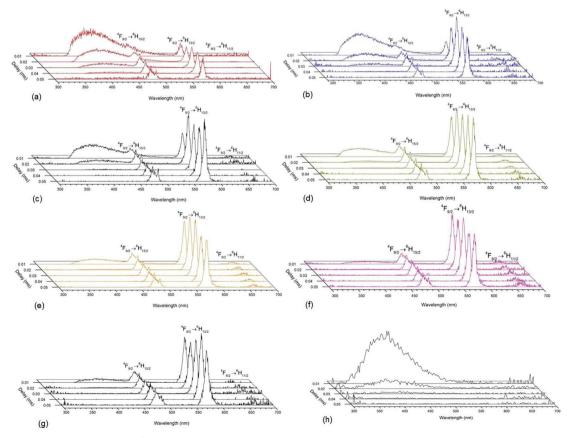

Figure 6. Time-resolved emission spectra (λ_{exc} = 254 nm) of the (Dy^{3+})-$LaNbO_4$ matrices with different Dy^{3+} concentrations: (a) 0.25%; (b) 0.5%; (c) 1.0%; (d) 3.0%; (e) 5.0%; (f) 10.0%; (g) 15.0% and (h) undoped sample.
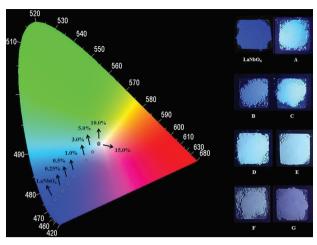
Figure 7. CIE coordinates of the samples containing different Dy^{3+} concentrations, excited at 254 nm. Inset: pictures of standard matrix undoped (LaNbO$_4$) and all samples under UV excitation (samples containing 0.25, 0.5, 1.0, 3.0, 5.0, 10.0 and 15.0% in moles of Dy^{3+} ion were called A, B, C, D, E, F and G, respectively).

Table 1. CIE coordinates and quantum yield of the samples containing different Dy^{3+} concentrations, excited at 254 nm

Dy^{3+} ions / %	CIE coordinates	
	x	y
Undoped sample	0.154	0.106
0.25	0.189	0.189
0.5	0.218	0.222
1.0	0.245	0.251
3.0	0.298	0.310
5.0	0.322	0.337
10.0	0.345	0.363
15.0	0.345	0.364

diminished the matrix emission band which allowed the tunable emission color by the combination of host and Dy^{3+} emissions. Furthermore, the CIE chromaticity coordinate obtained in this work suggest that these materials could be used as a single white-emitting phosphor in the solid-state white light emitters.

Acknowledgments

References

1. Serra, O. A.; de Lima, J. F.; de Sousa Filho, P. C.; *Rev. Virtual Quim.* **2015**, *7*, 242.

2. Saltarelli, M.; Luz, P. P.; Matos, M. G.; de Faria, E. H.; Ciuffi, K. J.; Calefi, P. S.; Rocha, L. A.; Nassar, E. J. ; *J. Fluoresc.* **2012**, *22*, 899.

3. Rocha, L. A.; Ciuffi, K. J.; Sacco, H. C.; Nassar, E. J.; *Mater. Chem. Phys.* **2004**, *85*, 245.

4. Matos, M. G.; de Faria, E. H.; Rocha, L. A.; Calefi, P. S.; Ciuffi, K. J.; Nassar, E. J.; Sarmento, V. H. V.; *J. Lumin.* **2014**, *147*, 190.

5. Santos, J. G.; Dutra, J. D. L.; Alves, S.; de Sá, G. F.; da Costa, N. B.; Freire, R. O.; *J. Braz. Chem. Soc.* **2013**, *24*, 236.

6. Liu, X.; Pang, R.; Li, Q.; Lin, J.; *J. Solid State Chem.* **2007**, *180*, 1421.

7. Binnemans, K.; *Coord. Chem. Rev.* **2015**, *295*, 1.

8. Blasse, G.; Brixner, L. H.; *Chem. Phys. Lett.* **1990**, *173*, 409.

9. Huang, J.; Zhou, L.; Liang, Z.; Gong, F.; Han, J.; Wang, R.; *J. Rare Earths* **2010**, *28*, 356.

10. Hsiao, Y. J.; Fang, T. H.; Chang, Y. S.; Chang, Y. H.; Liu, C. H.; Ji, L. W.; Jywe, W. Y.; *J. Lumin.* **2007**, *126*, 866.

11. Jian, L.; James, R. D.; *Acta Mater.* **1997**, *45*, 4271.

12. Mokkelbost, T.; Lein, H. L.; Vullum, P. E.; Holmestad, R.; Grande, T.; Einarsrud, M.-A.; *Ceram. Int.* **2009**, *35*, 2877.

13. Syvertsen, G. E.; Magrasó, A.; Haugsrud, R.; Einarsrud, M.-A.; Grande, T.; *Int. J. Hydrogen Energy* **2012**, *37*, 8017.

14. Freiria, G. S.; Nassar, E. J.; Verelst, M.; Rocha, L. A.; *J. Lumin.* **2016**, *169*, 844.

15. Li, K.; Zhang, Y.; Li, X.; Shang, M.; Lian, H.; Lin, J.; *Phys. Chem. Chem. Phys.* **2015**, *17*, 4283.

16. Sommerdijk, J. L.; *J. Electrochem. Soc.* **1975**, *122*, 952.

17. Zhang, X.; Meng, F.; Wei, H.; Seo, H. J.; *Ceram. Int.* **2013**, *39*, 4063.

18. Balamurugan, C.; Lee, D.-W.; Subramania, A.; *Appl. Surf. Sci.* **2013**, *283*, 58.

19. Amsif, M.; Marrero-López, D.; Ruiz-Morales, J. C.; Savvin, S.; Núñez, P.; *J. Eur. Ceram. Soc.* **2012**, *32*, 1235.

20. Xiao, X.; Yan, B.; *J. Alloys Compd.* **2006**, *421*, 252.

21. Matias, C. R.; Nassar, E. J.; Verelst, M.; Rocha, L. A.; *J. Braz. Chem. Soc.* **2015**, *26*, 2558.

22. Freiria, G. S.; Nassar, E. J.; Verelst, M.; Rocha, L. A.; *J. Lumin.* **2015**, *169*, 844.

23. Rocha, L. A.; Caiut, J. M. A.; Messaddeq, Y.; Ribeiro, S. J. L.; Martines, M. A. U.; Freiria, J. C.; Dexpert-Ghys, J.; Verelst, M.; *Nanotechnology* **2010**, *21*, 155603.

24. Brinker, C. J.; Lu, Y.; Sellinger, A.; Fan, H.; *Adv. Mater.* **1999**, *11*, 579.

25. Baccile, N.; Grosso, D.; Sanchez, C.; *J. Mater. Chem.* **2003**, *13*, 3011.

26. Sun, X.-Y.; Zhang, J.-C.; Liu, X.-G.; Lin, L.-W.; *Phys. B (Amsterdam, Neth.)* **2011**, *406*, 4089.

27. Sun, X.-Y.; Zhang, J.-C.; Liu, X.-G.; Lin, L.-W.; *Ceram. Int.* **2012**, *38*, 1065.

28. Venkata Rao, K.; Babu, S.; Venkataiah, G.; Ratnakaram, Y. C.; *J. Mol. Struct.* **2015**, *1094*, 274.

29. Li, L.; Li, R.; Zi, W.; Gan, S.; *Phys. B (Amsterdam, Neth.)* **2015**, *458*, 8.

30. Pereira, P. F. S.; Matos, M. G.; Ferreira, C. M. A.; de Faria, E. H.; Calefi, P. S.; Rocha, L. A.; Ciuffi, K. J.; Nassar, E. J.; *J. Lumin.* **2014**, *146*, 394.

31. Lennox, R. C.; Price, M. C.; Jamieson, W.; Jura, M.; Daoud-Aladine, A.; Murray, C. A.; Tang, C.; Arnold, D. C.; *J. Mater. Chem. C* **2014**, *2*, 3345.

32. Han, L.; Xie, X.; Lian, J.; Wang, Y.; Wang, C.; *J. Lumin.* **2016**, *176*, 71.

33. Wang, Z.; Li, P.; Yang, Z.; Guo, Q.; Li, X.; Teng, F.; *J. Rare Earths* **2015**, *33*, 1137.

34. Huang, C.-H.; Chen, T.-M.; *J. Phys. Chem. C* **2011**, *115*, 2349.

35. Rocha, L. A.; Freiria, J. C.; Caiut, J. M. A.; Ribeiro, S. J. L.; Messaddeq, Y.; Verelst, M.; Dexpert-Ghys, J.; *Nanotechnology* **2015**, *26*, 335604.

36. Momma, K.; Izumi, F.; *J. Appl. Crystallogr.* **2011**, *44*, 1272.

37. Nico, C.; Monteiro, T.; Graça, M. P. F.; *Prog. Mater. Sci.* **2016**, *80*, 1.

38. Rooksby, H. P.; White, E. A. D.; *Acta Crystallogr.* **1963**, *16*, 888.

39. Boldish, S. I.; White, W. B.; *Spectrochim. Acta, Part A* **1979**, *35*, 1235.

40. Cui, J.; Hope, G. A.; Cui, J.; Hope, G. A.; *J. Spectrosc.* **2015**, *2015*, article ID 940172.

41. Zhang, H.; Yang, Q.; Zhang, B.; Lu, S.; *J. Raman Spectrosc.* **2011**, *42*, 1384.

42. Palatnikov, M.; Shcherbina, O.; Sidorov, N.; Bormanis, K.; *Ukr. J. Phys. Opt.* **2012**, 207.

43. Ramarao, S. D.; Murthy, V. R. K.; *Phys. Chem. Chem. Phys.* **2015**, *17*, 12623.

44. Rocha, L. A.; Caiut, J. M. A.; Messaddeq, Y.; Ribeiro, S. J. L.; Martines, M. A. U.; Freiria, J. C.; *Nanotechnology* **2010**, *21*, 155603.

45. Liu, S.; Liang, Y.; Tong, M.; Yu, D.; Zhu, Y.; Wu, X.; Yan, C.; *Mater. Sci. Semicond. Process.* **2015**, *38*, 266.

46. Wang, T.; Hu, Y.; Chen, L.; Wang, X.; He, M.; *J. Lumin.* **2017**, *181*, 189.

47. Mahesh, S. K.; Rao, P. P.; Francis, T. L.; Reshmi, V. R.; Koshy, P.; *Mater. Lett.* **2014**, *120*, 115.

48. Kodaira, C. A.; Brito, H. F.; Felinto, M. C. F. C.; *J. Solid State Chem.* **2003**, *171*, 401.

49. Wang, T.; Hu, Y.; Chen, L.; Wang, X.; He, M.; *J. Lumin.* **2017**, *181*, 189.

50. Bang, H.; Morishima, S.; Sawahata, J.; Seo, J.; Takiguchi, M.; Tsunemi, M.; Akimoto, K.; Nomura, M.; *Appl. Phys. Lett.* **2004**, *85*, 227.

51. Ogugua, S. N.; Shaat, S. K. K.; Swart, H. C.; Ntwaeaborwa, O. M.; *J. Lumin.* **2016**, *179*, 154.

52. Santa-Cruz, P. A.; Teles, F. S.; *Spectra Lux Software*, Ponto Quantico Nanodispositivos, Recife, Brazil, 2003.

53. Vijayakumar, R.; Venkataiah, G.; Marimuthu, K.; *J. Alloys Compd.* **2015**, *652*, 234.

Submitted: June 2, 2017
Published online: September 25, 2017